CrossMark

Stability field diagrams for *Ln*–O–Cl systems

K T JACOB*, APOORVA DIXIT and ARNEET RAJPUT

Department of Materials Engineering, Indian Institute of Science, Bangalore 560012, India

Abstract. Isothermal stability field diagrams for *Ln*−O−Cl systems (*Ln* = La, Ce, Pr, Nd, Sm, Eu, Gd, Tb, Dy, Ho, Er, Tm, Yb) are developed by taking partial pressures of volatile components oxygen and chlorine as variables. Thermodynamic properties of all the oxides and trichlorides (*Ln*Cl$_3$) are available in the literature. However, data for oxychlorides (*Ln*OCl) and dichlorides (*Ln*Cl$_2$) are limited. Based on systematic trends in stability of these compounds across the lanthanide series, missing data are estimated to construct the diagrams for 13 *Ln*−O−Cl systems at 1000 K. All the lanthanide elements form stable *Ln*Cl$_3$ and *Ln*OCl. Dichlorides of Nd, Sm, Eu, Dy, Tm and Yb are stable. For systems in which dichlorides are unstable (*Ln* = La, Ce, Pr, Gd, Tb, Ho, Er), the *Ln*OCl is in equilibrium with the metal (*Ln*) and the stability field of *Ln*OCl is sandwiched between those of oxides and trichlorides. Stability field diagrams of lanthanide systems forming stable *Ln*Cl$_2$ are of two kinds: in the first kind (*Ln* = Nd, Dy) the stability fields of *Ln* and *Ln*OCl are in contact and the stability field of *Ln*OCl separates the fields of chlorides and oxides. In diagrams of the second kind (*Ln* = Sm, Eu, Tm, Yb) there is a direct equilibrium between the oxides and dichlorides at low partial pressures of oxygen and chlorine. There is no contact between the stability fields of *Ln* and *Ln*OCl; the stability field of *Ln*OCl intervenes between the oxide and chloride phases only at higher partial pressures.

Keywords. Predominance area diagram; Kellogg diagram; lanthanide oxychloride; rare-earth mineral processing; thermodynamic properties.

1. Introduction

There is an anticipated global shortage in supply of lanthanide resources because of the increasing use of lanthanide elements in a variety of advanced technologies, ranging from magnets to catalysts to phosphors [1], and the high Herfindahl–Hirschman index for production (HHI$_P$ = 9000) reflecting geopolitics [2,3]. Hence, there is general interest in recycling used products containing lanthanide metals and compounds. The conventional process for the extraction of lanthanide elements from oxide ores involves carbochlorination [4], although other chlorinating agents such as HCl and CCl$_4$ are also being tried [5]. In the conversion of most lanthanide oxides to chlorides, oxychloride phase forms as an intermediate product and controls the kinetics of the reaction, a fact recognized only in the recent literature. In the pyrochemical processing of spent nuclear fuels using molten salts, lanthanide elements are present as chlorides in the melt. They can be precipitated as oxychlorides or oxides by oxidation, either using solid oxidizing agents or sparging with oxygen gas [6]. Potential new processes involve the chlorination of lanthanides using AlCl$_3$ or MgCl$_2$ as chlorinating agents in a fused salt medium. The process yields lanthanide chloride or oxychloride, depending on the conditions of chlorination. The chloride dissolves fully in the molten salt, and the lanthanide elements can be recovered by electrolysis. The

presence of oxychloride with higher melting point complicates the process.

Doped tetragonal lanthanide oxychlorides are interesting materials for up-conversion of infrared light to visible. LaOCl is a good host for the smaller lanthanide ions. When LaOCl is co-doped with Er^{3+} and Yb^{3+} ions, it can produce strong green and red up-conversion emission at 526, 548 and 671 nm on excitation by a 980 nm diode laser [7]. LaOCl:Eu^{2+} is a blue-emitting phosphor [8]. The lighter *Ln*OCl (*Ln* = La to Ho) compounds crystallize in the tetragonal PbFCl-type structure, space group *P*4/*nmm*. The structure can be visualized as layers of distinct covalent (*Ln*O)$_n^{n+}$ complex cations and Cl$^-$ anions. The metal atom is coordinated to four oxygen atoms and five chlorine atoms in a monocaped tetragonal antiprism arrangement [9]. The Cl$^-$ ions come into an unusually close contact with each other. As the size of the lanthanide decreases, the deformation of Cl$^-$ ions increases and the structure becomes unstable. A few heavier *Ln*OCl (*Ln* = Tm to Lu) compounds have SmSI-type rhombohedral structure, space group *R*$\bar{3}$*m* [10]. In this structure the metal atom is coordinated to four oxygen atoms and four chlorine atoms. The volume occupied by hexagonal *Ln*OCl is much smaller than that of the tetragonal variety. ErOCl is dimorphic.

Unfortunately, thermodynamic data for only four *Ln*OCl compounds (*Ln* = La, Nd, Sm, Gd) are available in thermodynamic data compilations [11] and phase diagrams of *Ln*−O−Cl systems are nonexistent. Information on the

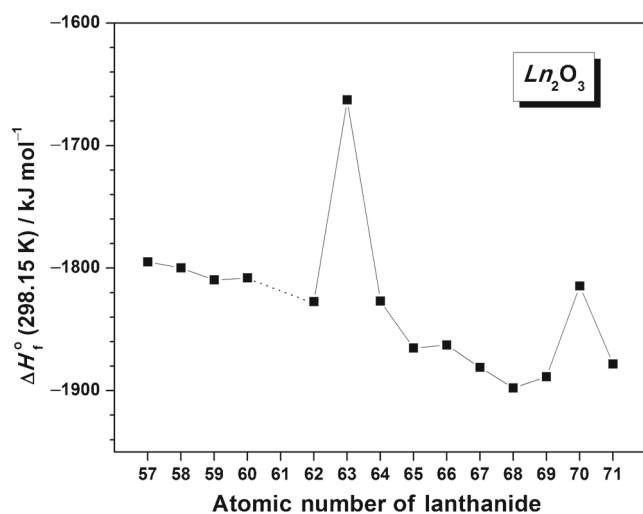stability domains of various phases in all $Ln-O-Cl$ systems is useful for the design and optimization of processes involving the conversion of lanthanide oxides to chlorides or vice versa. The purpose of this communication is to gather data on LnOCl compounds, estimate missing information and construct stability field diagrams, which would be useful for assessing the feasibility of new processes.
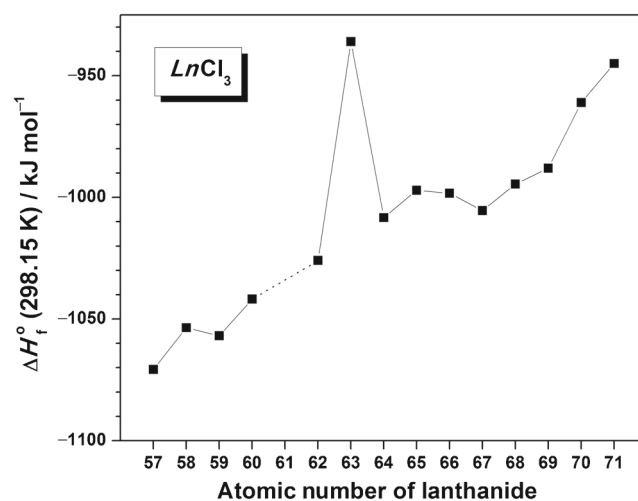
2. Thermodynamic data

Comprehensive thermodynamic data for lanthanide sesquioxides (Ln_2O_3), trichlorides (LnCl$_3$) and two dichlorides (Ln = Sm, Yb) are given in the compilation of Knacke *et al* [11] at regular intervals of temperature. The enthalpy of formation of the oxide at 298.15 K is shown as a function of atomic number in figure 1. The stability of Ln_2O_3 increases with atomic number, except for Eu and Yb. The divalent state of these two elements associated with half and completely filled 4f shell is more stable than the trivalent state, and promotion energy is required in forming trivalent compounds. The trichlorides (LnCl$_3$) become less stable with increase in atomic number as shown in figure 2. The melting point of LnCl$_3$ decreases almost linearly with atomic number from 1131 K for LaCl$_3$ to 853 K for TbCl$_3$ and then increases monotonically to 1198 K for LuCl$_3$. The trichlorides of elements from La to Gd have hexagonal UCl$_3$-type structure. TbCl$_3$ exhibits a phase transition at 790 K with crystal structure changing from orthorhombic PuBr$_3$-type to orthorhombic trirutile-type. DyCl$_3$ transforms from low temperature monoclinic (AlCl$_3$-type) to orthorhombic (PuBr$_3$ type) at 611 K. The subsequent lanthanides (Ho to Lu) have monoclinic AlCl$_3$-type structure [12]. The different general trends in the variation of stability of Ln_2O_3 and LnCl$_3$ compounds provide a tool for the separation of lanthanides.

The stability of the oxychlorides (LnOCl) decreases marginally with atomic number with Eu and Yb as exceptions,

as seen in figure 3. The data for oxychlorides are less accurate than the data of oxides and trichlorides. For four elements (Ln = La, Nd, Sm and Gd) thermodynamic data for oxychlorides as a function of temperature are provided in the compilation of Knacke *et al* [11]. Burns *et al* [13] measured enthalpy of formation of three lanthanide oxychlorides (Ln = Eu, Gd and Lu) by solution calorimetry in 1 N hydrochloric acid at 298.15 K. Based on these results and other information available in the literature, Burns *et al* [13] estimated the enthalpies of formation for all lanthanide oxychlorides (LnOCl). Gibbs energy of formation of oxychloride LnOCl at high temperature (1000 K) was estimated using an average value for the entropy change for the solid-state reaction, $(1/3)Ln_2O_3 + (1/3)Ln$Cl$_3 \rightarrow Ln$OCl ($\Delta S_{av} = -8$ (± 4) J mol^{-1} K^{-1}) and invoking the Neumann-Kopp rule to estimate the heat capacity of oxychlorides. In all systems, the oxychloride is found to be stable.

Figure 2. Standard enthalpy of formation of trichlorides at 298.15 K as a function of atomic number.

Figure 1. Standard enthalpy of formation of sesquioxides at 298.15 K as a function of atomic number.
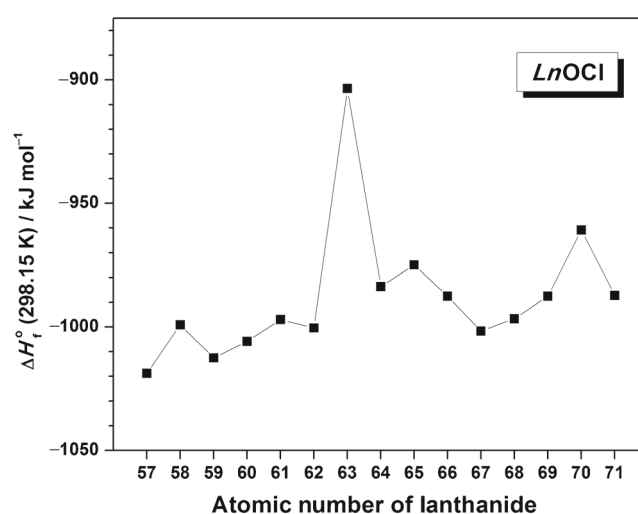
Figure 3. Standard enthalpy of formation of oxychlorides at 298.15 K as a function of atomic number.

Table 1. Summary of thermodynamic data used for construction of stability field diagrams at 1000 K.

Atomic number	Chemical symbol	ΔG_f° (Ln_2O_3) (kJ mol^{-1})	ΔG_f° (other lanthanide oxides) (kJ mol^{-1})	ΔG_f° ($LnCl_2$) (kJ mol^{-1})	ΔG_f° ($LnCl_3$) (kJ mol^{-1})	ΔG_f° ($LnOCl$) (kJ mol^{-1})
57	La	−1508.842 (a)			−829.3025 (a)	−836.839 (a)
58	Ce	−1512.87 (a)	CeO_2 : −882.378 (a)		−811.5925 (a)	−814.316 (d)
59	Pr	−1518.582 (a)	Pr_7O_{12}: −5399.511 (a)		−814.7055 (a)	−825.608 (d)
60	Nd	−1524.974 (a)		−541.154 (c)	−801.7315 (a)	−806.675 (a)
62	Sm	−1530.688 (a)		−658.213 (a)	−780.8185 (a)	−821.645 (a)
63	Eu	−1355.068 (a)	EuO: −494.152 (a) Eu_3O_4: −1864.64 (e)	−666.219 (c)	−689.3295 (a)	−710.739 (d)
64	Gd	−1538.825 (a)			−773.5055 (a)	−801.814 (a)
65	Tb	−1578.41 (a)	Tb_7O_{12}: −5556.72 (a)		−762.1265 (a)	−793.823 (d)
66	Dy	−1565.825 (a)		−559.224 (c)	−753.8365 (a)	−798.554 (d)
67	Ho	−1591.563 (a)			−759.9815 (a)	−814.465 (d)
68	Er	−1606.756 (b)			−752.0525 (a)	−808.824 (d)
69	Tm	−1584.005 (a)		−580.569 (c)	−748.3545 (a)	−797.224 (d)
70	Yb	−1530.423 (a)		−645.694 (a)	−709.7605 (a)	−772.335 (d)
71	Lu	−1585.374 (a)				

(a): Knacke *et al* [11]; (b): Pankratz [16,17]; (c): Uda *et al* [15]; (d): Burns *et al* [13]; (e): Jacob and Rajput [21].

Data for two lanthanide dichlorides ($LnCl_2$; Ln = Sm, Yb) are available in the literature [11]. In addition, dichlorides of Nd, Eu, Dy and Tm are known to be stable according to Meyer *et al* [14]. Values for dichlorides estimated by Uda *et al* [15] are used. For reactions of the type $Ln + Cl_2 \rightarrow LnCl_2$ and $2LnCl_2 + Cl_2 \rightarrow 2LnCl_3$, involving one mole of Cl_2 gas, the entropy change was taken to be −175 (±10) J mol^{-1} K^{-1}. All the data used for constructing stability field diagrams are summarized in table 1. Thermodynamic data for Ce_3O_5, Ce_7O_{12} and PrO_2 are not available in standard thermodynamic compilations [11,16,17]. The oxygen potentials for the oxidation of Ce_2O_3 to Ce_3O_5, Ce_3O_5 to Ce_7O_{12} and Ce_7O_{12} to CeO_2 are taken from a thermodynamic assessment of the phase diagram for the Ce-O system [18]. The oxygen potential for the oxidation of Pr_7O_{12} to PrO_{2-x} is taken from tensimetric measurements of Kordis and Eyring [19].

3. Stability field diagrams and discussion

Application of phase rule to ternary $Ln-O-Cl$ system at constant temperature indicates that the system is invariant when three condensed phases coexist with a gas phase. Hence, partial pressures of oxygen and chlorine are uniquely defined. Isothermal stability field diagram is a plot of the logarithm of partial pressures of chlorine and oxygen in the gas phase. Such a diagram is also known as predominance−area diagram or Kellogg diagram. On this plot, equilibrium between three condensed phases will be denoted by an invariant point. The equilibrium involving two condensed phases and the gas phase will have one degree of freedom and therefore will be represented by a line. A single condensed phase in equilibrium with a gas will have two degrees of freedom and is represented on the diagram by an area.
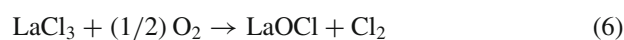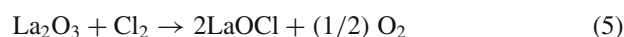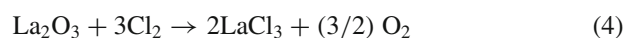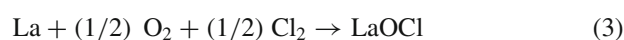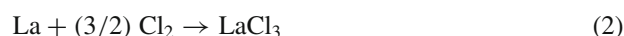
If the number of condensed phases in $Ln-O-Cl$ system is n, there will be $^nC_2$ combinations of condensed phases, each of which can be represented by a line on the stability field diagram. Not all combinations of condensed phases will be in equilibrium. The equilibrium combination can be identified by minimization of free energy. The lines representing equilibrium combinations of condensed phases define the stability field diagram.

Some of the lanthanides (Ln = La, Ce, Pr, Gd, Tb, Ho, Er) form trichloride ($LnCl_3$) as the only stable chloride, while others (Ln = Nd, Sm, Eu, Dy, Tm, Yb) form both dichloride ($LnCl_2$) and trichloride ($LnCl_3$) as stable compounds. For convenience, stability field diagrams for Ln–O–Cl systems can be grouped into two categories: systems that do not form stable dichlorides and systems that form both dichlorides and trichlorides.
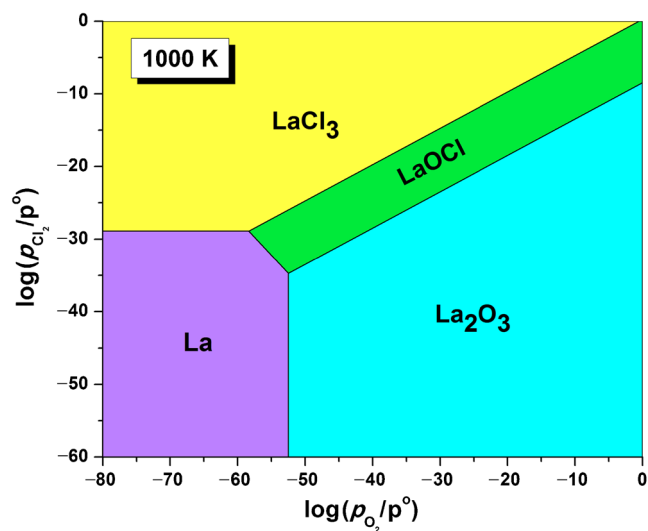
Category 1: $Ln-O-Cl$ systems with unstable dichlorides:

Of the lanthanides that form only trichlorides, La, Gd, Ho and Er form only one stable oxide (Ln_2O_3). Multiple oxide phases exist for Ce (Ce_2O_3, Ce_3O_5, Ce_7O_{12}, CeO_{2-x}), Pr (Pr_2O_3, Pr_7O_{12}, PrO_{2-x}) and Tb (Tb_2O_3, Tb_7O_{12}).

For the La−O−Cl system we have the following set of possible reactions:

$$2La + (3/2)\, O_2 \rightarrow La_2O_3 \tag{1}$$

$$La + (3/2)\, Cl_2 \rightarrow LaCl_3 \tag{2}$$

$$La + (1/2)\, O_2 + (1/2)\, Cl_2 \rightarrow LaOCl \tag{3}$$

$$La_2O_3 + 3Cl_2 \rightarrow 2LaCl_3 + (3/2)\, O_2 \tag{4}$$

$$La_2O_3 + Cl_2 \rightarrow 2LaOCl + (1/2)\, O_2 \tag{5}$$

$$LaCl_3 + (1/2)\, O_2 \rightarrow LaOCl + Cl_2 \tag{6}$$

Since the Gibbs energy of formation of lanthanum oxychloride from sesquioxide and trichloride (((1/3) La_2O_3 + (1/3) $LaCl_3$ → $LaOCl$) is negative, the sesquioxide cannot coexist with the trichloride. Along the pseudo-binary La_2O_3−$LaCl_3$ system there exists two subsolidus biphasic regions La_2O_3 + $LaOCl$ and $LaOCl$ + $LaCl_3$ on either side of the oxychloride. Hence, reaction (4) does not represent true equilibrium. The stability field diagram for La−O−Cl computed from thermodynamic data, listed in table 1, is displayed as figure 4. At very low oxygen and chlorine partial pressures the stable phase is metal La. On increasing oxygen pressure, La_2O_3 forms according to reaction (1) at $\log(p_{O_2}/p^o) = -52.5$, where $p^o = 0.1$ MPa is the standard pressure. The boundary between the metal and oxide is a vertical line independent of chlorine partial pressure. On increasing chlorine pressure over La metal, $LaCl_3$ forms according to reaction (2) at $\log(p_{Cl_2}/p^o) = -28.9$. The boundary between metal and trichloride is a horizontal line independent of oxygen partial pressure. The formation of LaOCl from La metal, oxygen and chlorine is governed by reaction (3). When metal and oxychloride are in equilibrium, the product of partial pressures of oxygen and chlorine is a constant. The line with a slope of -1 defines a boundary between these phases, which intersects the La−$LaCl_3$ and La−La_2O_3 boundaries as shown in figure 4.

The boundary line between La_2O_3 and $LaOCl$, defined by the reaction (5), with a slope of 0.5 meets the boundary lines between La−La_2O_3 and La−$LaOCl$, and the point of intersection represents invariant equilibrium involving the three phases La, La_2O_3 and $LaOCl$. Similarly, the boundary line between $LaCl_3$ and $LaOCl$, defined by the reaction (6), with a slope of 0.5 meets the boundary lines between La−$LaCl_3$ and La−$LaOCl$, and the point of intersection marks another invariant point where the three phases La, $LaCl_3$ and $LaOCl$ coexist. The vertical distance between La_2O_3−$LaOCl$ and

$LaOCl$−$LaCl_3$ lines or the width of the oxychloride stability field is a measure of the Gibbs energy of formation of the oxychloride from sesquioxide and trichloride.

It can be seen from the diagram that neither the oxide can be converted to chloride nor the chloride can be converted to oxide without the formation of the oxychloride. Since the melting point of the oxychloride is significantly higher than that of the chloride, it would normally precipitate from the halide melts during processing. Only a partial phase diagram for the $LaCl_3$−$LaOCl$ system is available, which shows eutectic at 1093 K [20].

Stability field diagrams for Gd−O−Cl (figure 5), Ho−O−Cl (figure 6) and Er−O−Cl (figure 7) systems at 1000 K are very similar to that for La−O−Cl. Elements Ce, Pr and Tb form multiple oxides. As a result, a set of reactions in addition to reactions of the type (1) to (6) has to be
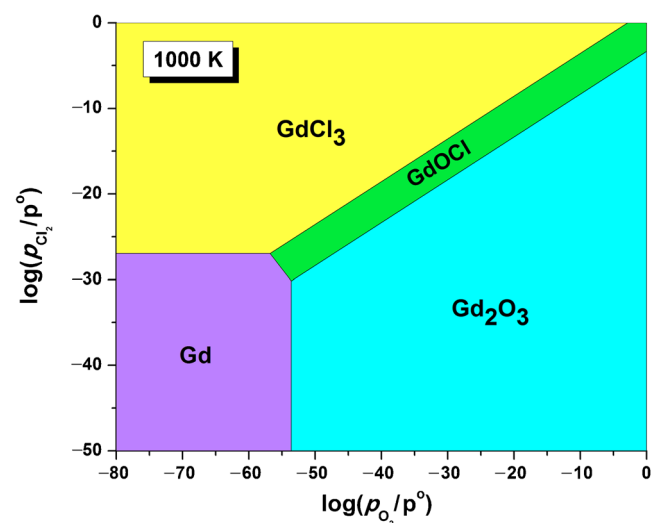
Figure 5. Stability field diagram for the Gd−O−Cl system at 1000 K.

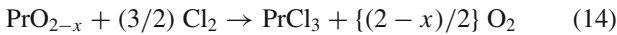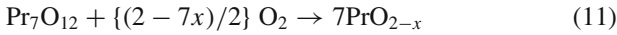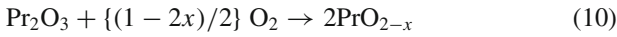**Figure 4.** Stability field diagram for the La−O−Cl system at 1000 K.
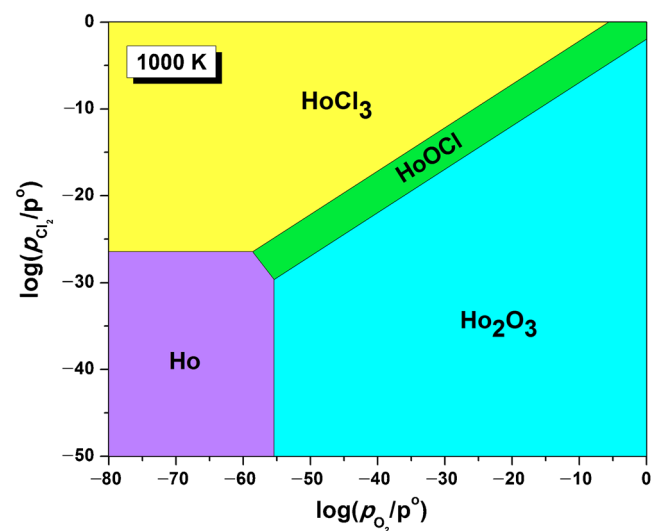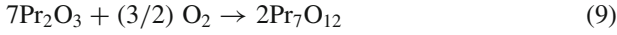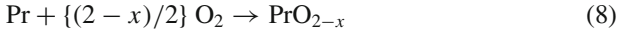
Figure 6. Stability field diagram for the Ho−O−Cl system at 1000 K.
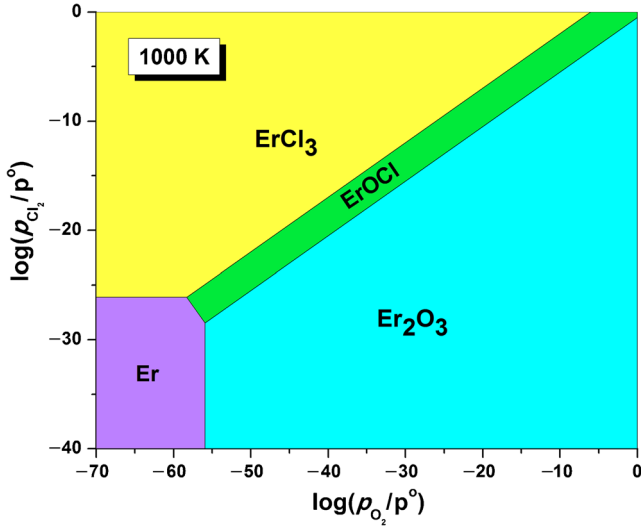
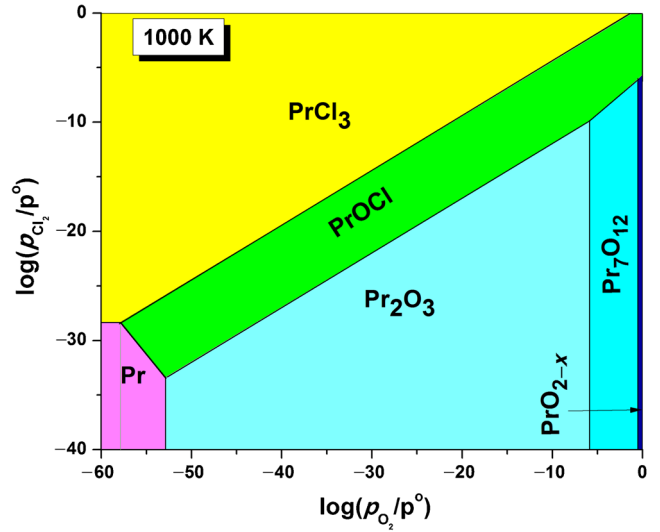**Figure 7.** Stability field diagram for the Er−O−Cl system at 1000 K.

Figure 8. Stability field diagram for the Pr−O−Cl system at 1000 K.

considered. For the Pr−O−Cl system, because of the presence of higher oxides Pr_7O_{12} and $PrO_{2−x}$ the additional reactions are as follows:

$$7Pr + 6O_2 \rightarrow Pr_7O_{12} \tag{7}$$

$$Pr + \{(2 − x)/2\} O_2 \rightarrow PrO_{2−x} \tag{8}$$

$$7Pr_2O_3 + (3/2) O_2 \rightarrow 2Pr_7O_{12} \tag{9}$$

$$Pr_2O_3 + \{(1 − 2x)/2\} O_2 \rightarrow 2PrO_{2−x} \tag{10}$$

$$Pr_7O_{12} + \{(2 − 7x)/2\} O_2 \rightarrow 7PrO_{2−x} \tag{11}$$

$$Pr_7O_{12} + (21/2) Cl_2 \rightarrow 7PrCl_3 + 6O_2 \tag{12}$$

$$Pr_7O_{12} + (7/2) Cl_2 \rightarrow 7PrOCl + (5/2) O_2 \tag{13}$$

$$PrO_{2−x} + (3/2) Cl_2 \rightarrow PrCl_3 + \{(2 − x)/2\} O_2 \tag{14}$$

$$PrO_{2−x} + (1/2) Cl_2 \rightarrow PrOCl + \{(1 − x)/2\} O_2. \tag{15}$$

The stability field diagram for Pr−O−Cl computed from thermodynamic data, listed in table 1, is shown as figure 8. Reactions (7), (8), (10), (12) and (14) do not represent true equilibrium since Pr_2O_3 forms between Pr and Pr_7O_{12}, Pr_7O_{12} between Pr_2O_3 and $PrO_{2−x}$, and PrOCl forms between the higher oxides and $PrCl_3$. On increasing oxygen pressure over the metal, first Pr_2O_3 forms according to reaction similar to (1) at $\log(p_{O_2}/p^o) = −52.9$. On further increasing the oxygen pressure, Pr_7O_{12} starts to form according to reaction (9) at $\log(p_{O_2}/p^o) = −5.9$ and $PrO_{2−x}$ according to reaction (11) at $\log(p_{O_2}/p^o) = −0.519$. The average value of the nonstoichiometric parameter x in the narrow stability range of $PrO_{2−x}$ at 1000 K is 0.21 [19]. The boundary lines between Pr and Pr_2O_3, and Pr_7O_{12} and $PrO_{2−x}$ are vertical. The boundary between Pr and $PrCl_3$ is a horizontal line at $\log(p_{Cl_2}/p^o) = −28.4$. The Pr and PrOCl

equilibrium line (slope = −1) intersects the Pr−Pr_2O_3 and Pr_2O_3−PrOCl boundaries forming an invariant point, where three phases Pr, Pr_2O_3 and PrOCl coexist as shown in figure 8. The second invariant point (Pr−$PrCl_3$−PrOCl) is generated by the intersection of Pr−PrOCl boundary with Pr−$PrCl_3$ and $PrCl_3$−PrOCl lines. These two invariant points are similar to those that exist in case of *Ln*−O−Cl (*Ln* = La, Gd, Ho and Er). The additional features in the Pr−O−Cl system arise from the presence of Pr_7O_{12} and $PrO_{2−x}$ as stable phases. The boundary between Pr_7O_{12} and PrOCl (slope = 5/7) is given by the reaction (13), which intersects the equilibrium lines between Pr_2O_3−Pr_7O_{12} and Pr_2O_3−PrOCl to form the third invariant point (Pr_2O_3−Pr_7O_{12}−PrOCl). The fourth invariant point is generated by the intersection of the three lines corresponding to the equilibria Pr_7O_{12}−$PrO_{2−x}$, Pr_7O_{12}−PrOCl and $PrO_{2−x}$−PrOCl (slope = (1–x) = 0.79). Figure 8 shows that none of the oxides can be directly converted to chloride without the formation of PrOCl. The stability field diagram for Tb−O−Cl at 1000 K, presented in figure 9, is similar to that for Pr−O−Cl. The stability of Tb^{4+} state is because of its half filled f shell ($4f^7$).

Since Ce^{4+} ion has inert gas [Xe] configuration, nonstoichiometric $CeO_{2−x}$ is formed as a stable oxide at higher oxygen partial pressures in addition to Ce_7O_{12}, nonstoichiometric Ce_3O_5 and Ce_2O_3 which are stable at lower oxygen chemical potentials. The stability field diagram for Ce−O−Cl system constructed following the procedures outlined earlier is displayed as figure 10. On increasing the oxygen pressure over metallic Ce initially Ce_2O_3 is formed at $\log(p_{O_2}/p^o) = −52.7$, followed by Ce_3O_5 at $\log(p_{O_2}/p^o) = −29.47$, Ce_7O_{12} at $\log(p_{O_2}/p^o) = −28.91$ and finally $CeO_{2−x}$ at $\log(p_{O_2}/p^o) = −27.82$. There are six invariant points in the stability field diagram for the Ce−O−Cl system. The first two (Ce−Ce_2O_3−CeOCl) and (Ce−$CeCl_3$−CeOCl) are similar to those encountered in the
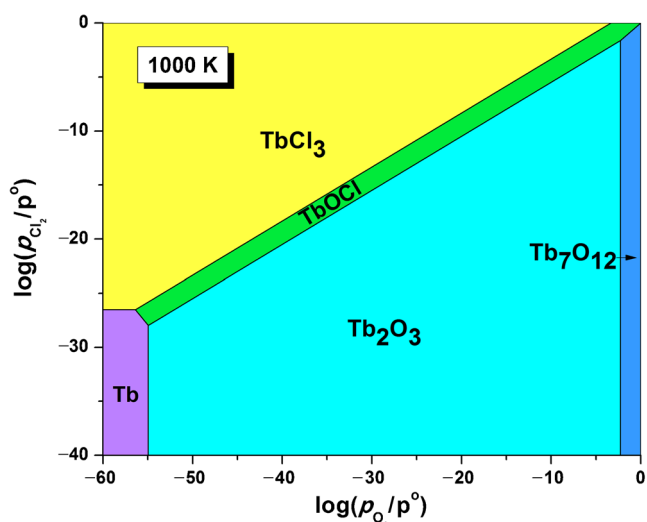
Figure 9. Stability field diagram for the Tb−O−Cl system at 1000 K.
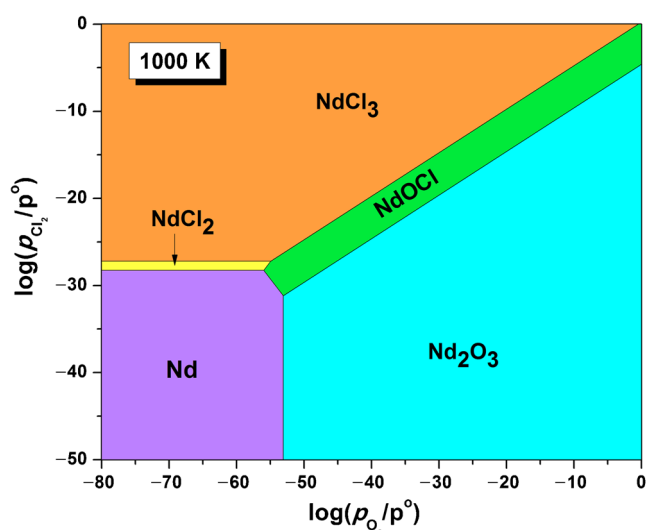
Figure 11. Stability field diagram for the Nd−O−Cl system at 1000 K.
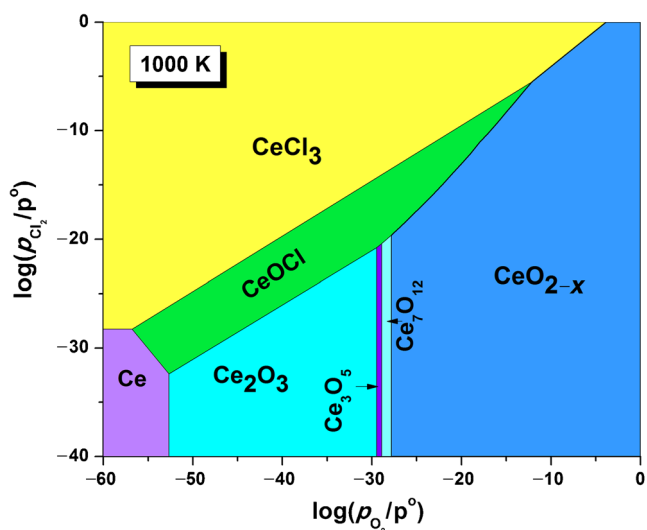
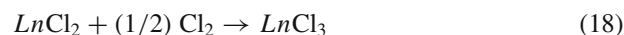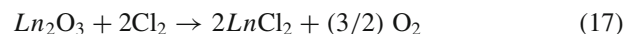**Figure 10.** Stability field diagram for the Ce−O−Cl system at 1000 K.

earlier diagrams. The boundary line between Ce_2O_3 and CeOCl (slope = 1/2) intersects Ce_2O_3−Ce_3O_5 (vertical) and Ce_3O_5−CeOCl (slope = 5/7) lines, resulting in the formation of a third invariant point (Ce_2O_3−Ce_3O_5−CeOCl). Likewise, the boundary line between Ce_3O_5−CeOCl intersects Ce_3O_5−Ce_7O_{12} (vertical) and Ce_7O_{12}−CeOCl (slope = 5/7) boundary lines, resulting in the formation of a fourth invariant point (Ce_3O_5−Ce_7O_{12}−CeOCl). The fifth invariant point corresponds to the equilibrium between Ce_7O_{12}, CeO_{2-x} and CeOCl. A large nonstoichiometric range characterizes CeO_{2-x} at 1000 K, $0 \leq x \leq 0.23$. Because of large change in oxygen stoichiometry with oxygen partial pressure, the boundary line between CeO_{2-x} and CeOCl has a small curvature. The limiting slope of this line at the Ce_7O_{12}−CeO_{2-x}−CeOCl invariant point is $(1–x) = 0.77$. The limiting slope of this boundary at the sixth invariant

point CeO_{2-x}−CeOCl−$CeCl_3$ is 0.99. The invariant point is defined by $\log(p_{O_2}/p^o) = -12.12$ and $\log(p_{Cl_2}/p^o) = -5.50$. Beyond this invariant point, at higher partial pressures of oxygen and chlorine, there is a line representing the equilibrium between CeO_2 and $CeCl_3$. Among the systems having trichloride as the only stable chloride, Ce−O−Cl is the only system where direct conversion of CeO_2 to $CeCl_3$ (and vice versa) is possible under controlled conditions.

Category 2: *Ln*−O−Cl systems having stable dichlorides and trichlorides:

Both dichlorides ($LnCl_2$) and trichlorides ($LnCl_3$) are stable in many *Ln*−O−Cl (*Ln* = Nd, Sm, Eu, Dy, Tm, Yb) systems. All these elements except Eu forms only one stable oxide (Ln_2O_3). Eu forms three stable oxides: EuO, Eu_3O_4 and Eu_2O_3.

Because of the presence of dichloride, in addition to reactions (1) to (6) with La replaced by *Ln*, following set of reactions involving $LnCl_2$ have to be considered:

$$Ln + Cl_2 \rightarrow LnCl_2 \tag{16}$$

$$Ln_2O_3 + 2Cl_2 \rightarrow 2LnCl_2 + (3/2)\ O_2 \tag{17}$$

$$LnCl_2 + (1/2)\ Cl_2 \rightarrow LnCl_3 \tag{18}$$

$$LnCl_2 + (1/2)\ O_2 \rightarrow LnOCl + (1/2)\ Cl_2. \tag{19}$$

Depending on the stability domain of the dichloride, category 2 systems can be further subdivided into two types:

Type 1: In diagrams of type 1 (*Ln* = Nd, Dy), the stability fields of *Ln* and *Ln*OCl are in contact and the stability field of *Ln*OCl separates the fields of both chloride phases from that of the oxide. In these systems, stability field of the dichloride is very small and therefore the presence of dichloride does not significantly alter the topology of the diagram.

Stability field diagram of Nd−O−Cl at 1000 K is shown in figure 11. The lines for reactions of type (2), (4) and

(17) are not shown, as these do not denote true equilibrium. On increasing the chlorine pressure over Nd, $NdCl_2$ forms at $\log(p_{Cl_2}/p^o) = -28.3$ according to reaction (16) and then converts to $NdCl_3$ according to reaction (18) at $\log(p_{Cl_2}/p^o) = -27.2$. Thus a narrow stability field of $NdCl_2$ forms between those of Nd and $NdCl_3$. The presence of $NdCl_2$ introduces a new line with slope unity, corresponding to $NdCl_2-NdOCl$ equilibrium governed by reaction (19). Three invariant points ($Nd-Nd_2O_3-NdOCl$), ($Nd-NdCl_2-NdOCl$) and ($NdCl_2-NdCl_3-NdOCl$) are encountered in the diagram. The stability field of NdOCl intervenes between those of Nd_2O_3 and $NdCl_3$, and Nd_2O_3 and $NdCl_2$. Therefore the chlorides cannot be directly converted to oxide and vice versa. $Dy-O-Cl$ system (figure 12) is a limiting case, where the oxychloride phase field makes a point contact with the metal (Dy) phase.

Type 2: In type 2 systems ($Ln =$ Sm, Eu, Tm, Yb), the stability field of the dichloride is larger resulting in direct equilibrium between the oxide and dichloride at low partial pressures of oxygen and chlorine. There is no contact between the stability fields of *Ln* and *Ln*OCl; *Ln*OCl intervenes between the oxide and chloride phases only at higher partial pressures of oxygen and chlorine.
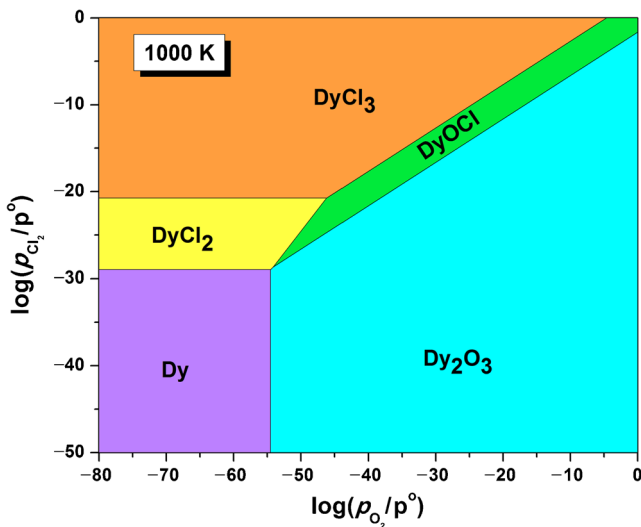
The stability field diagram for $Sm-O-Cl$ system at 1000 K is presented as figure 13. Reactions (2), (3) and (4) do not represent true equilibrium, as $SmCl_2$ forms between Sm and $SmCl_3$, $SmCl_2$ and Sm_2O_3 intervenes between Sm and SmOCl, and SmOCl forms between Sm_2O_3 and $SmCl_3$. On rising chlorine pressure over metal, it forms $SmCl_2$ at $\log(p_{Cl_2}/p^o) = -34.4$ according to reaction (15) and subsequently converts to $SmCl_3$ according to reaction (17) at $\log(p_{Cl_2}/p^o) = -12.8$. There are three invariant points in the diagram. First one ($SmCl_2-SmCl_3-SmOCl$) results from the intersection of equilibrium lines $SmCl_2-SmCl_3$ (slope $= 0$, reaction (18)), $SmCl_2-SmOCl$ (slope $= 1$, reaction (19)) and $SmCl_3-SmOCl$ (slope $= 0.5$, reaction (6)). A

new feature here is that there is an equilibrium line between Sm_2O_3 and $SmCl_2$ (reaction (17)), hence they can be converted to each other at low values of p_{O_2} and p_{Cl_2}. However, at higher partial pressures oxychloride intervenes between oxide and chloride phases, because of which oxide and chloride cannot be directly inter-converted. The equilibrium line between Sm_2O_3 and $SmCl_2$ intersects lines for $Sm-SmCl_2$ and $Sm-Sm_2O_3$ equilibria, forming second invariant point ($Sm-Sm_2O_3-SmCl_2$). The third invariant point represents equilibrium between $SmCl_2$, Sm_2O_3 and SmOCl. In a similar manner, diagrams for $Tm-O-Cl$ (figure 14) and $Yb-O-Cl$ (figure 15) systems are developed.

The $Eu-O-Cl$ system has EuO and Eu_3O_4 as additional oxide phases. Stability field diagram for $Eu-O-Cl$ system at 1000 K composed from thermodynamic data is shown as figure 16. On increasing the oxygen partial
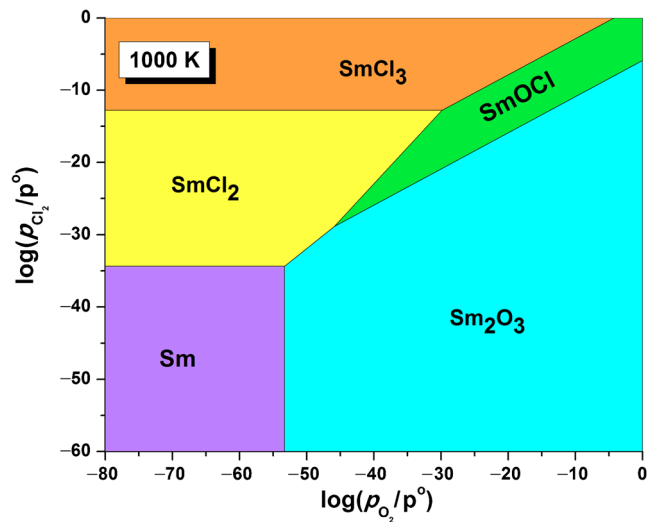
Figure 13. Stability field diagram for the $Sm-O-Cl$ system at 1000 K.
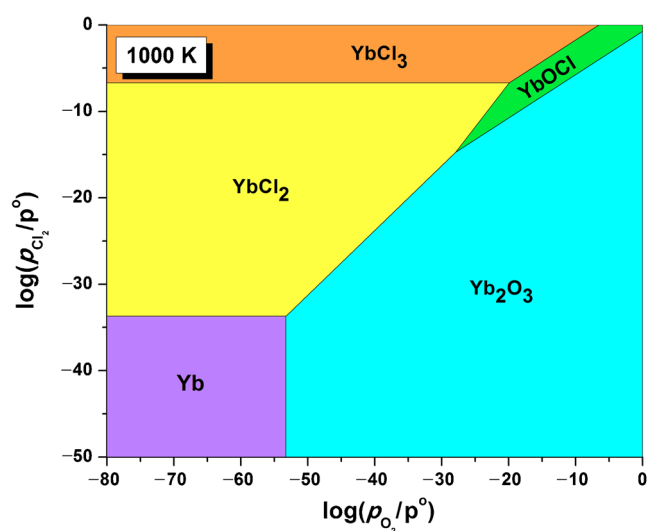

Figure 12. Stability field diagram for the $Dy-O-Cl$ system at 1000 K.
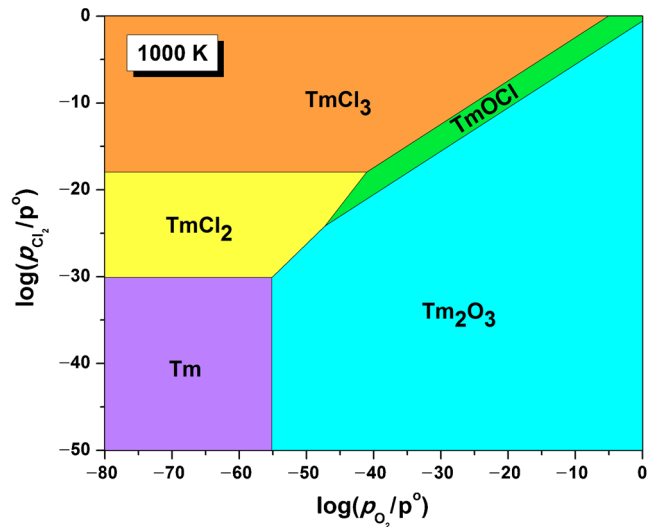
Figure 14. Stability field diagram for the $Tm-O-Cl$ system at 1000 K.

pressure over metal, the oxides EuO, Eu_3O_4 and Eu_2O_3 are produced sequentially at $\log(p_{O_2}/p^o) = -51.6, -39.9$ and -35.1. The stability field of Eu_3O_4 is smaller compared to those of EuO and Eu_2O_3. On increasing chlorine pressure over the metal, $EuCl_2$ and $EuCl_3$ are obtained according to reactions (16) and (18) at $\log(p_{Cl_2}/p^o) = -34.6$ and -2.9, respectively. The large stability field of $EuCl_2$ is an important feature of this diagram. All the oxides are in equilibrium with dichloride. There are five invariant points $(Eu-EuO-EuCl_2)$, $(EuO-Eu_3O_4-EuCl_2)$, $(Eu_3O_4-Eu_2O_3-EuCl_2)$, $(Eu_2O_3-EuCl_2-EuOCl)$ and $(EuCl_2-EuCl_3-EuOCl)$, all of which involve $EuCl_2$. The stability field of EuOCl occurs at relatively higher partial pressures of oxygen and chlorine; EuOCl is in contact with Eu_2O_3, $EuCl_2$ and $EuCl_3$. The diagram shows that there is a large thermodynamic window for the direct conversion of oxides to dichloride and vice versa.

4. Three-dimensional chemical potential diagram

The stability field diagram is essentially a projection of phase relations in the ternary system onto a 2-D plane that portrays chemical potentials or partial pressure of the two volatile components (oxygen and chlorine) that can be independently controlled. To describe the complete stability domain of a ternary phase, chemical potentials of all three components must be defined along the boundaries of the domain. In the stability field diagrams presented in this communication, the chemical potential of the lanthanide element is not shown. A 3-D chemical potential diagram for the system La−O−Cl at 1000 K is shown in figure 17. Chemical potential of the three elements of this system is chosen as variables. In this diagram, the stability domain of each phase is shown as a plane. For example, the stability domain of La−O−Cl system is defined by the Gibbs energy of formation of the compound:

$$\Delta G_f^o \,(\text{LaOCl}) = -\Delta\mu_{\text{LaOCl}} + \Delta\mu_{\text{La}} + 1/2\Delta\mu_{O_2} + 1/2\Delta\mu_{Cl_2}. \tag{20}$$

Since LaOCl is present as a pure phase at the unit activity, its chemical potential is zero. It follows from the equation that slope of the plane is determined by the stoichiometry of the compound. Similarly, the stability domain of other phases can be calculated using the Gibbs energy of formation of the respective compound given in table 1. If a non-stoichiometric phase exists, then it would be represented by a curved surface in the 3-D diagram. The intersection of two planes or surfaces defines a two-phase region. Points of intersection of three planes define three-phase equilibrium.

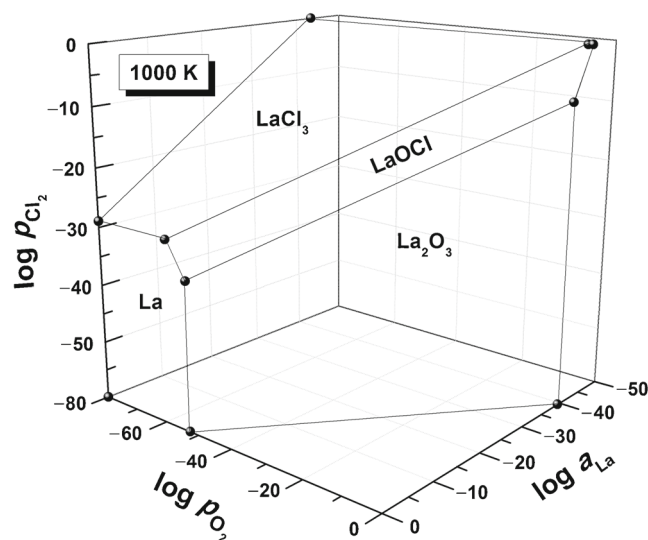

Figure 15. Stability field diagram for the Yb−O−Cl system at 1000 K.

Figure 16. Stability field diagram for the Eu−O−Cl system at 1000 K.

Figure 17. Three-dimensional chemical potential diagram for the La−O−Cl system at 1000 K.

5. Conclusions

This article presents a panoramic view of the evolution of phase relations in the $Ln-O-Cl$ systems (Ln = lanthanide element). The diagrams are constructed at 1000 K. However, the thermodynamic data allow construction of such diagrams at any desired temperature. The diagrams show that it is possible to convert lanthanide sesquioxides directly to lanthanide chloride only when the lanthanide dichloride has a large stability domain; the direct conversion is confined to low oxygen and chlorine partial pressures. In systems where dichloride is unstable, lanthanide oxychloride will form as a stable phase between the sesquioxide and trichloride phases. The formation of oxychloride as an intermediate phase will affect the kinetics of chlorination of lanthanide oxides to their corresponding chlorides. Only in the case of Ce, it is possible to convert CeO_2 directly to $CeCl_3$ at high oxygen and chlorine partial pressures. If lanthanide elements are present in the chloride melt as in pyroprocessing of spent nuclear fuels, they can be precipitated as oxychlorides and oxides by oxidation.

Acknowledgements

References

[1] Rambabu U, Mathur A and Bhuddhudu S 1999 *Mater. Chem. Phys.* **61** 156

[2] Rosenau-Tornow D, Buchholz P, Riemann A and Wagner M 2009 *Resour. Policy* **34** 161

[3] Gaultois M W, Sparks T D, Borg C K H, Seshadri R, Bonificio W D and Clarke D R 2013 *Chem. Mater.* **25** 2911

[4] Gimenes M A and Oliveira H P 2001 *Metall. Mater. Trans. B* **32B** 1007

[5] Augusto E B and Oliveira H P 2001 *Metall. Mater. Trans. B* **32B** 785

[6] Cho Y J, Yang H C, Eun H C, Kim E H and Kim J H 2005 *J. Ind. Eng. Chem.* **11** 707

[7] Kong Q, Wang J, Dong X, Yu W and Liu G 2014 *J. Mater. Sci.* **49** 2919

[8] Kim D, Jang J, Ahn S I, Kim S H and Park J C 2014 *J. Mater. Chem. C* **2** 2799

[9] Brixner L H and Moore E P 1983 *Acta Crystallogr. C* **39** 1316

[10] Brandt G and Diehl R 1974 *Mater. Res. Bull.* **9** 411

[11] Knacke O, Kubaschewski O and Hesselmann K 1991 *Thermochemical properties of inorganic substances* (Berlin: Springer-Verlag) 2nd edn

[12] Gaune-Escard M 2005 *Scand. J. Metall.* **34** 369

[13] Burns J B, Peterson J R and Haire R G 1998 *J. Alloys Compd.* **265** 146

[14] Meyer G 1988 *Chem. Rev.* **88** 93

[15] Uda T, Jacob K T and Hirasawa M 2000 *Science* **289** 2326

[16] Pankratz L B 1982 *Thermodynamic properties of elements and oxides* Bulletin 674 (Washington: United States Bureau of Mines)

[17] Pankratz L B 1984 *Thermodynamic properties of halides* Bulletin 674 (Washington: United States Bureau of Mines)

[18] Zinkevich M, Djurovic D and Aldinger A 2006 *Solid State Ionics* **177** 989

[19] Kordis J and Eyring L 1968 *J. Phys. Chem.* **72** 2044

[20] Drobot D V, Korshunov B G and Durinina L V 1965 *Inorg. Mater.* **1** 1978

[21] Jacob K T and Rajput A 2016 *J. Chem. Eng. Data*, doi: 10.1021/acs.jced.5b00728